

The Relationship between Boron Content and Crack Properties in FCAW Deposited Metal

Cold cracking in thick steel plate welding is investigated as a function of boron contents

BY H. W. LEE

ABSTRACT. This study has evaluated the susceptibility of the deposited weld metal to cold cracking as a function of boron content. The panels were welded with three different boron content electrodes (2% Ni flux cored wire) with the flux cored arc welding (FCAW) process.

Cracks were not detected for the specimens welded with 32- and 60-ppm boron content electrodes, while cracks were detected for the specimen welded with 103 ppm boron content electrode. Diffusible hydrogen contents were 3~4 mL per 100 g of deposited weld metal, and most diffusible hydrogen escaped within 2 h after welding. The cracks were observed 45 deg to the longitudinal direction of the weld joint. From optical microscopy, it was determined that the cracks propagated across the grains and grain boundary.

Introduction

The various cracks that can occur in weld joints, depending on welding conditions and processes, are classified as cold crack and hot crack according to occurrence temperatures. Hot cracking, such as solidification cracks and liquation cracks, are the most severe problems associated with the partially melted zone (PMZ). The cause of hot cracking in the PMZ is the combination of grain boundary liquation and stresses induced by both solidification shrinkage and thermal contraction during welding (Refs. 1, 2).

The cold crack generally occurs at temperatures below 200°C, either immediately upon cooling or after a period of several hours. The time delay depends upon the type of steel, the magnitude of the welding stresses, and the hydrogen content of the weld (Refs. 3-5). The cause of cold cracking is diffusible hydrogen, hardened microstructure, and residual stresses; such cracking is called hydrogen-assisted cracking. There are two types of

hydrogen cracking in a heat-affected zone (HAZ) or weld metal: 1) that occurring during welding and 2) that occurring during service. The latter is called stress corrosion cracking of the hydrogen embrittlement type, and it is caused by hydrogen entering into a weldment from moist hydrogen sulfide gas or other hydrogenous environments in service (Ref. 6). Hydrogen-induced cold cracking in the HAZ has been one of the problems in the welding of carbon manganese and low-alloy steels. It has been overcome by the introduction of better-quality steels with lower carbon content.

In fact, as the carbon content decreases toward 0.10 wt-% or less in the new steels, they tend to be free from the HAZ cracking problem. Cold cracking has become more prevalent in the deposited weld metal due to use of high-hydrogen consumables (Refs. 7, 8).

One apparently new type of cracking was identified during the late 1960s. It coincided with the then newly developed basic agglomerated fluxes for submerged arc welding (SAW). Due to the parallel pattern of the defects, it was designated chevron cracking, transverse 45 deg cracking, or staircase cracking; however, the first term is still the most widely used. The cracks are characterized by their orientation, which is approximately transverse to the welding direction and at 45 deg with the plane of the plate in a butt joint (Refs. 8, 9). For a given hydrogen content and residual stress, the hardened microstructure will lead to cold cracking.

Small amounts of boron in the weld

metal have a significant influence on the microstructure. Various mechanisms are proposed for boron hardenability in steels. One suggestion for boron hardenability is that free boron diffuses to austenite grain boundaries and lowers their energy, thereby making them less favorable sites for ferrite nucleation (Refs. 10, 11).

In this study, the cold cracking was studied as a function of boron content for the deposited weld metal.

Experimental Procedures

Test Panel/Welding

The size of the test panel was 2000 mm long x 1800 mm wide x 40 mm thick. The panel was fabricated from EH36 TMCP (thermomechanical controlled process) higher-strength hull steel.

Three sets of test panels were made without any external restraint conditions, as shown in Fig. 1, with the specimen sections welded in layers as shown in Fig. 2.

The panels were welded with three experimental Ti-Ni flux cored wires designed to produce systematic variations in the concentration of weld metal boron of 32, 60, and 103 ppm.

The panels were welded with the three electrodes, using the FCAW process with automatic carriage (1.4 mm diameter, 20 L/min flow rate, 100% CO₂ gas, electrode extension of 25-30 mm). Welding parameters are shown in Table 1.

Chemical Composition/Microstructure

The chemical analyses of the three welds were performed with a Baird Emission Spectrometer. The weld metal oxygen and nitrogen were determined using Leco Interstitial Analyzers. The chemical compositions of base and weld metals are shown in Table 2 and Table 3, respectively.

The specimens were prepared by polishing through one-micron alumina abrasive, followed by etching for 10-15 s in a solution of 2% Nital. A standard point counting technique was used to determine

KEYWORDS

FCAW
Boron Content
Crack
Diffusible Hydrogen
Residual Stresses

H. W. LEE (hwlee@hanjinsc.com) is with the Welding Research Team of Hanjin Heavy Industries, Busan City, Korea.

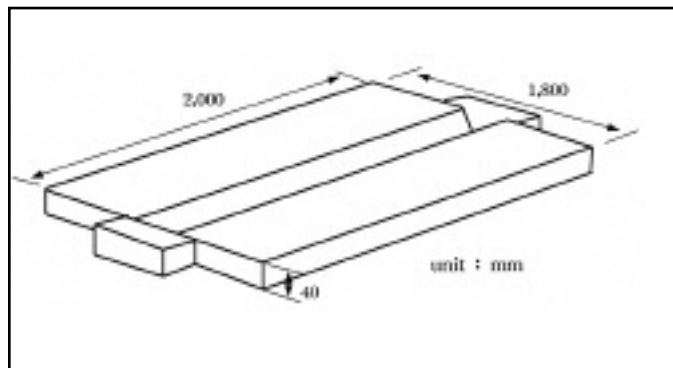


Fig. 1 — Schematic diagram of weld panel.

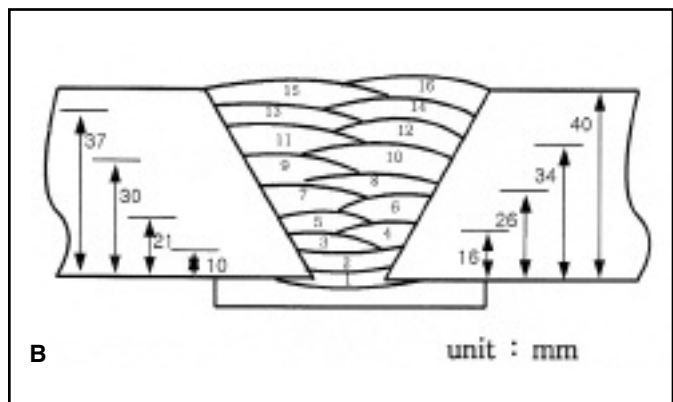
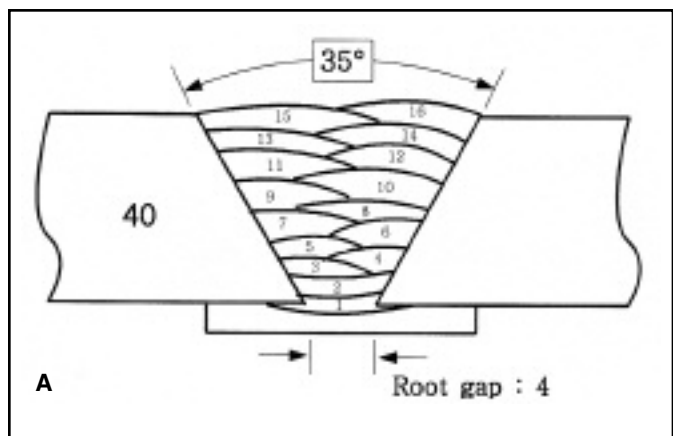


Fig. 2 — Schematic diagram of weld metal deposit.

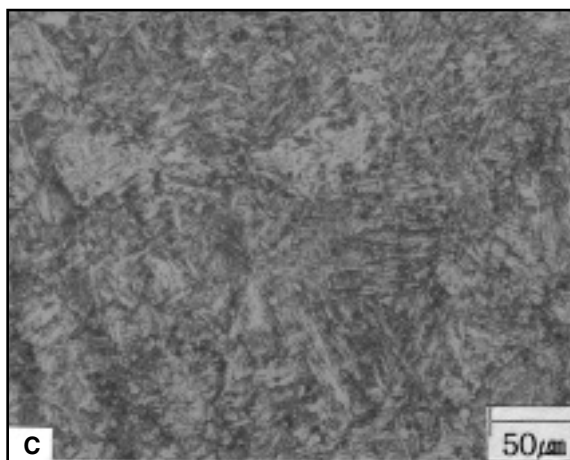
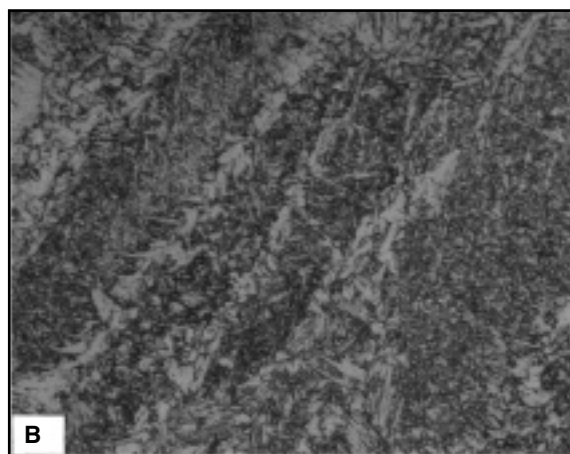
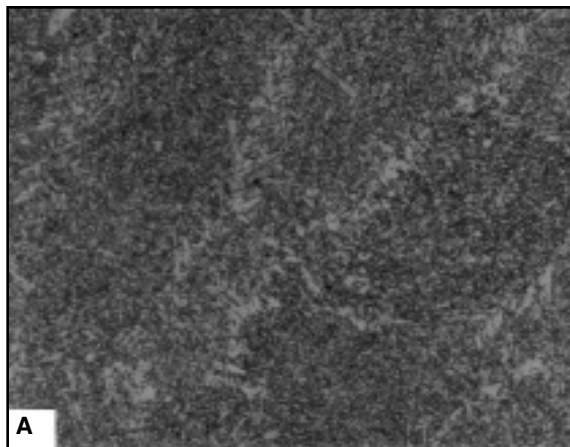


Fig. 3 — Microstructure of deposit metal as a function of boron content. A — 32 ppm; B — 60 ppm; and C — 103 ppm.

the volume fractions of acicular ferrite at a magnification of 500X. The microstructural constituents were classified based on the guidelines suggested by Pargeter and Dolby (Ref. 12).

Hardness

Hardness was measured using the macro Vickers hardness test, with a load of 5 kg and 10 s of loading time. Measurements were made on transverse sections 20 mm from the top surface.

Diffusible Hydrogen Test

The diffusible hydrogen was measured by the glycerin method per JIS Z3118. Before the hydrogen test, the steel plate was kept in the furnace at 500°C for 1 h and air cooled to remove diffusible hydrogen.

Result and Discussion

Microstructure

Figure 3 is an optical micrograph taken

from the deposited weld metal area as a function of boron content. Figure 3A is the microstructure of deposited weld metal welded with 32 ppm boron content electrode, and 3B is welded with 60 ppm boron content electrode. The optical microscopy revealed no significant difference in Fig. 3A and B, except for acicular ferrite content. The microstructures consisted of grain boundary ferrite, Widmanstatten side plate, and acicular ferrite. The volume fractions of acicular ferrite that is transformed from austenite de-

creased with increasing boron content from 32 to 62 ppm.

The acicular ferrite content in the specimen with 32 ppm boron was transformed approximately 93%, while the specimen with 60 ppm boron was transformed 87%. In contrast, the primary ferrite, such as grain boundary ferrite and Widmanstätten side plate, increased as boron content increased, as shown in Fig. 3A.

The microstructure of deposited weld metal welded with the 103 ppm boron content electrode is shown in Fig. 3C. The microstructure showed significant differences as compared to Fig. 3A and B. The bainite that transformed from austenite is shown in Fig. 3C.

Oh et al. (Ref. 13) proposed that the upper bainite content increases from 0 to 8% with increasing boron content from 6 to 91 ppm. The reduction in toughness with increasing boron concentration above the optimum content can be related to the role of bainite on the degradation of weld metal properties. It is expected that variations in hardenability additions, such as manganese and carbon, will cause changes in the boron and titanium contents that achieve the optimum amount of acicular ferrite and maximum toughness.'

Hardness Traverses

Figure 4 shows the hardness traverses 20 mm away from the weld surface.

The hardness values of the deposited weld metal revealed significant differences as a function of boron content. The hardness values of the welds produced with 32 and 60 ppm boron electrodes are HV 190~210, while those produced with the 103 ppm boron electrode are HV 230~235. The weld metal hardness values increased with increasing boron content.

Table 1 — Welding Parameters

Pass No.	Current (A)	Voltage (V)	Travel Speed (cm/min)	Heat input (J/cm)
1, 2	260	28	18	24
3-7	320	30	25	23
8-14	330	32	25	25
15, 16	320	31	22	27

Welding process	Flux cored arc welding
Welding position	Flat
Filler metal specification	A 5.29 E81T1-K2
Filler metal classification	DS 81-K2
Shielding gas/flow rate	CO ₂ (100%)
Electrode extension (mm)	25-30
Polarity	DCEP
Preheating/interpass temp.	50°C

One suggestion for boron hardenability is that free boron diffuses to austenite grain boundaries and lowers their energy, thereby making them less favorable sites for ferrite nucleation. Ohmori and Yamanaka (Ref. 14) have found evidence of grain boundary enrichment with high-sensitivity ion microprobe analysis.

Diffusible Hydrogen

Diffusible hydrogen generated under the welding arc at a significantly high temperature. The hydrogen dissolved in the weld metal is proportional to the square root of the partial pressure of the hydrogen gas. The following sources of weld metal hydrogen are considered in FCAW (Ref. 6):

1. Moisture in flux
2. Moisture in CO₂ gas
3. Organic substance in flux
4. Hydrogen in electrode steel and

steel plate

5. Moisture in atmosphere
6. Extraneous hydrogenous material, e.g., moisture, grease, and paint.

Hydrogen dissolved in a steel matrix is diffusible, thereby causing hydrogen embrittlement. The weld metal hydrogen content is generally expressed by the content of diffusible hydrogen. The three methods of measuring diffusible hydrogen contents are as follows:

1. Glycerin method (H_{JIS})
2. Mercury method (H_{IW})
3. Gas chromatography method (H_{GC}).

The test results of these three methods are related as follows:

$$H_{IW} = 1.27H_{JIS} + 2.19$$

$$H_{GC} = 2H_{JIS} + 0.3$$

where H_{IW}, H_{GC}, and H_{JIS} are the weld metal diffusible hydrogen content per 100 g of deposited weld metal. The hydrogen contents, which depend on welding conditions, were measured by the glycerin

Table 2 — Chemical Composition of Base Metal

	C	Si	Mn	P	S	Ni	Cr	Mo	V	Ti	TS (N/mm ²)	YS (N/mm ²)	EI (%)
EH32 TMCP (spec.)	0.18 max.	0.10 ~0.50	0.90 ~1.60	0.040 max.	0.040 max.	0.04 max.	0.02 max.	0.08 max.	0.10 max.	0.02 max.	440~590	310 min.	20.0
Base metal (experi.)	0.08	0.38	1.35	0.015	0.005	0.03	0.03	0.02	0.002	0.02	518	372	31.0

Table 3 — Chemical Composition of Weld Metals

	C (wt-%)	Si (wt-%)	Mn (wt-%)	P (wt-%)	S (wt-%)	Ni (wt-%)	Ti (wt-%)	B (ppm)	O (ppm)	N (ppm)
No. 1	0.02	0.55	1.41	0.010	0.006	1.85	0.050	32	284	126
No. 2	0.02	0.54	1.38	0.012	0.005	1.90	0.045	60	290	134
No. 3	0.02	0.54	1.40	0.010	0.005	1.87	0.048	103	276	142

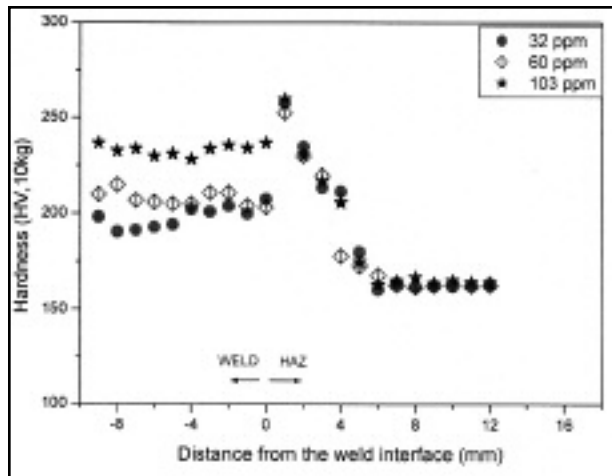


Fig. 4 — Hardness traverses as a function of boron content.

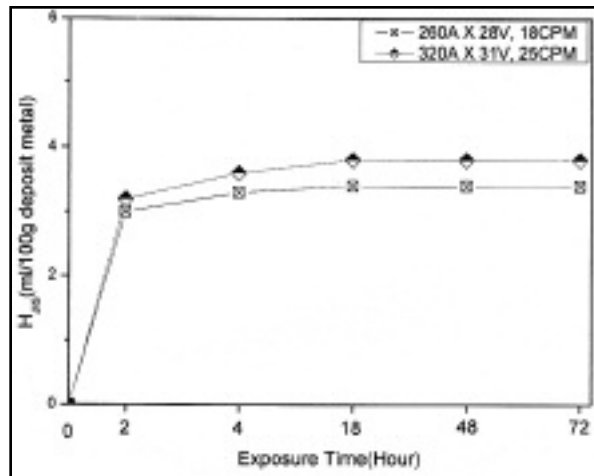


Fig. 5 — Hydrogen content profiles depending on welding conditions.

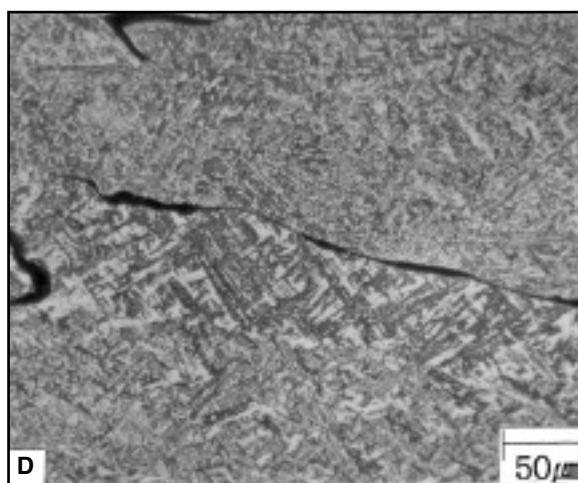
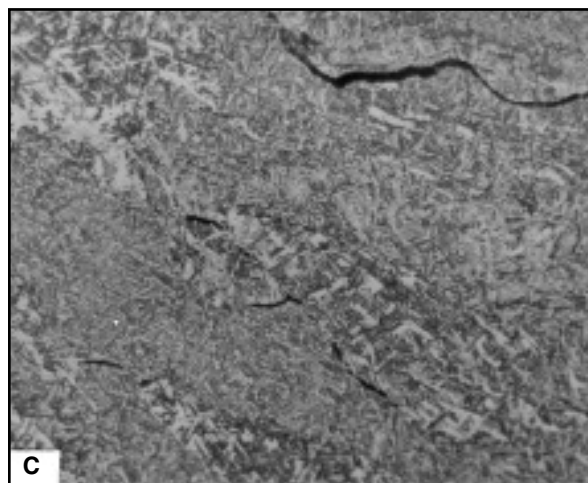
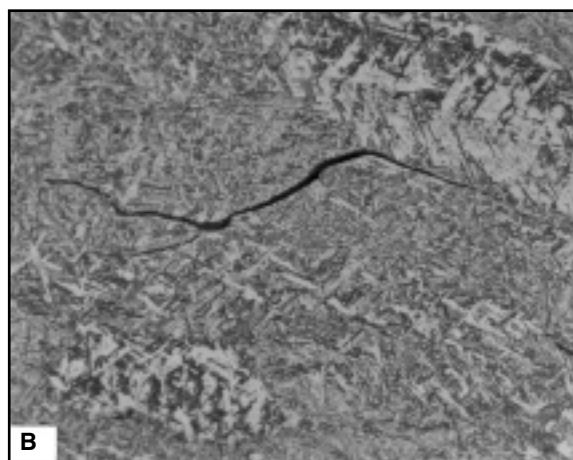
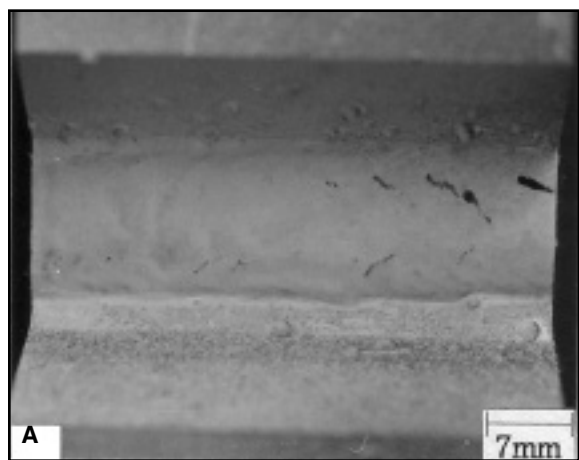


Fig. 6 — Various cracks in deposited weld metal welded with 103 ppm boron-content wire.

method and are shown in Fig. 5. These data indicate that welds made with the FCAW electrode have hydrogen contents of approximately 3~4 mL/100 g (6~8 mL/100 g for GC). Most diffusible hydrogen escaped within 2 h after welding as shown in Fig. 5. The diffusible hydrogen content increased with increasing welding

current and voltage; however, there were no significant hydrogen contents in the three electrodes.

Crack Morphology

In the joint welded with the 32 and 60 ppm boron content electrodes, no cracks

were detected. However, cracks were detected with the specimen welded with the 103 ppm boron content electrode. Based upon a number of oblique Y-groove root cracking tests of various high-strength steels, Ito and Bessyo (Ref. 15) proposed a cracking parameter, P_W , from which the critical preheating temperature, to avoid

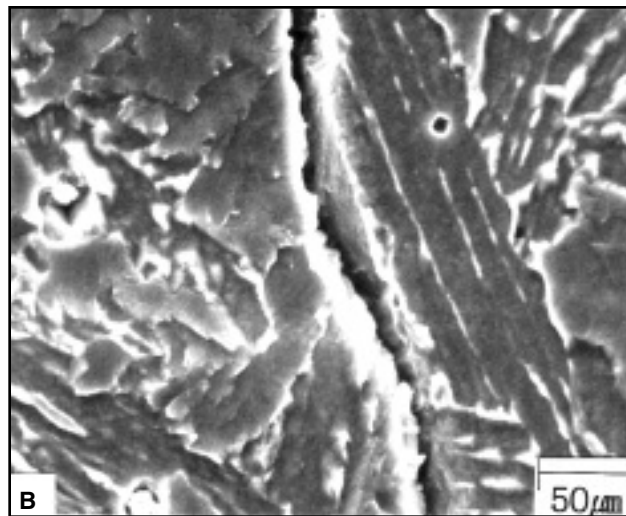
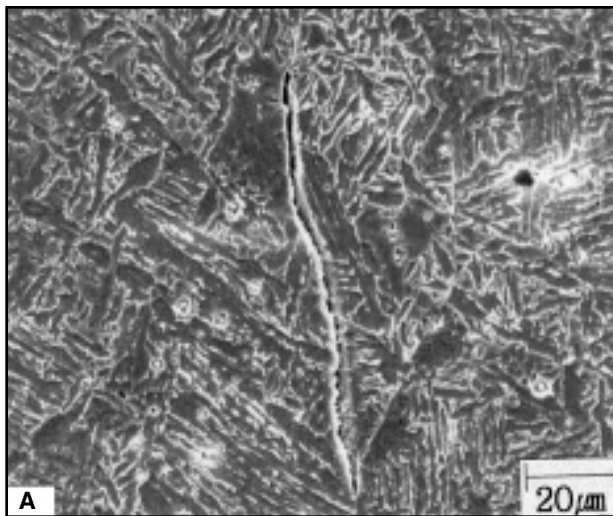


Fig. 7 — SEM microstructure of cracked area.

cracking, can be predicted before welding. The parameter is a linear combination of P_{cm} (cracking carbon equivalent), intensity of tensile restraint R_f (kg/mm²), and diffusible hydrogen content per 100 g of deposited weld metal H_D . The root cracking parameter (P_W) is

$$P_W = P_{cm} + H_D/60 + R_f/40000$$

where P_{cm} , root cracking carbon equivalent, calculated with chemical composition is

$$P_{cm} = C + Si/30 + (Mn+Cu+Cr)/20 + Ni/60 + Mo/15 + V/10 + 5B \quad (1)$$

It is noted that boron has the greatest effect on susceptibility to cold cracking according to Equation 1.

Figure 6A shows the results of magnetic particle inspection after three layers of welding. The cracks were observed 45 deg to the longitudinal section. These cracks are called chevron cracks, transverse 45-deg cracking, or staircase cracking; however, the term chevron crack is still the most widely used. Keville's theory (Ref. 16) suggested that the 45-deg cracking orientation coincides with the direction of maximum shear stress. The suggested mechanism of chevron cracking is as follows:

1. Longitudinal tensile stresses build up as the weld bead cools, and approach or exceed yield point magnitude. Plastic strain is initially concentrated in the soft intercolumnar proeutectoid ferrite. When enough hydrogen is present, the ductility of the proeutectoid ferrite is greatly reduced, and so an intercolumnar microcrack may nucleate.

2. As the crack grows, the size of the plastic zone at the crack tip will tend to increase. Hence, the crack may be blunted and arrested. The plastic zone may then form the nucleus of a long-range

transcolumnar shear band at 45 deg to the longitudinal direction.

3. Plastic flow within the shear band then leads to dislocation pileups at the neighboring columnar grain boundaries. The stress concentration at the head of the pileup nucleates a second, separate intercolumnar crack, either directly by causing decohesion at a weak zone such as an inclusion, or indirectly by promoting further plastic flow in the proeutectoid ferrite.

Diffusible hydrogen transport to the columnar grain boundary by moving dislocations assists crack formation.

4. The second intercolumnar crack, in turn, grows and blunts. In this way, an array of intercolumnar crack segments forms by repeated nucleation on columnar grain boundaries within the shear band.

5. The crack array forms a zone of weakness. This promotes further plastic flow between the microcrack tips. Horizontal transcolumnar cracks therefore form by ductile shear, assisted by hydrogen. These cracks link the intercolumnar microcracks together to produce a macrocrack.

Figure 6B–D shows optical micrographs of the crack morphology in the deposited weld metal. Also, the SEM fractographs of the opened crack area are shown in Fig. 7. The formation of these cracks propagated not only across grains (Fig. 6B), but also along grain boundaries (Fig. 6D). Lee et al. (Refs. 17, 18) have shown that in welds produced with magnified weld residual stresses in thick steel plate, the formation of cold cracks did not follow the grain boundary; rather, they propagated across the grains, and were detected in the area of maximum residual stresses

for both the SAW and FCAW processes.

In this study, the specimens were welded without any external restraint conditions, and the morphology of cracks differed from those of Lee's report. This is due to large restraint stresses under actual construction conditions, as compared to small restraint stresses. Microscopic fracture modes from the Beachem (Ref. 19) report are shown in Fig. 8. These illustrations show the tip of cracks growing under varying K (stress intensity factor) conditions, with the K decreasing from Fig. 8A–D.

Conclusions

The relationship between boron content and cold cracking was studied for EH36 TMCP 40-mm-thick plate welded with the FCAW process. The results of this study can be summarized as follows:

1. Cracks were detected in the specimen welded with the 103 ppm boron content electrode; however, cracks were not detected for the specimen welded with 32 and 60 ppm boron content electrodes.

2. Diffusible hydrogen contents were 3~4 mL per 100 g of deposited weld metal, and they increased with increasing welding current and voltage; however, the hydrogen content was not considered significant.

3. The cracks were observed 45 deg to the longitudinal direction of the weld joint.

4. From optical microscopy, it was determined that the cracks propagated across the grains and grain boundaries.

References

1. Kou, S. 1987. *Welding Metallurgy*. New York, N.Y.: John Wiley and Sons, pp. 249, 326.
2. *Welding Handbook*. 1987. 8th ed., Vol. 1,

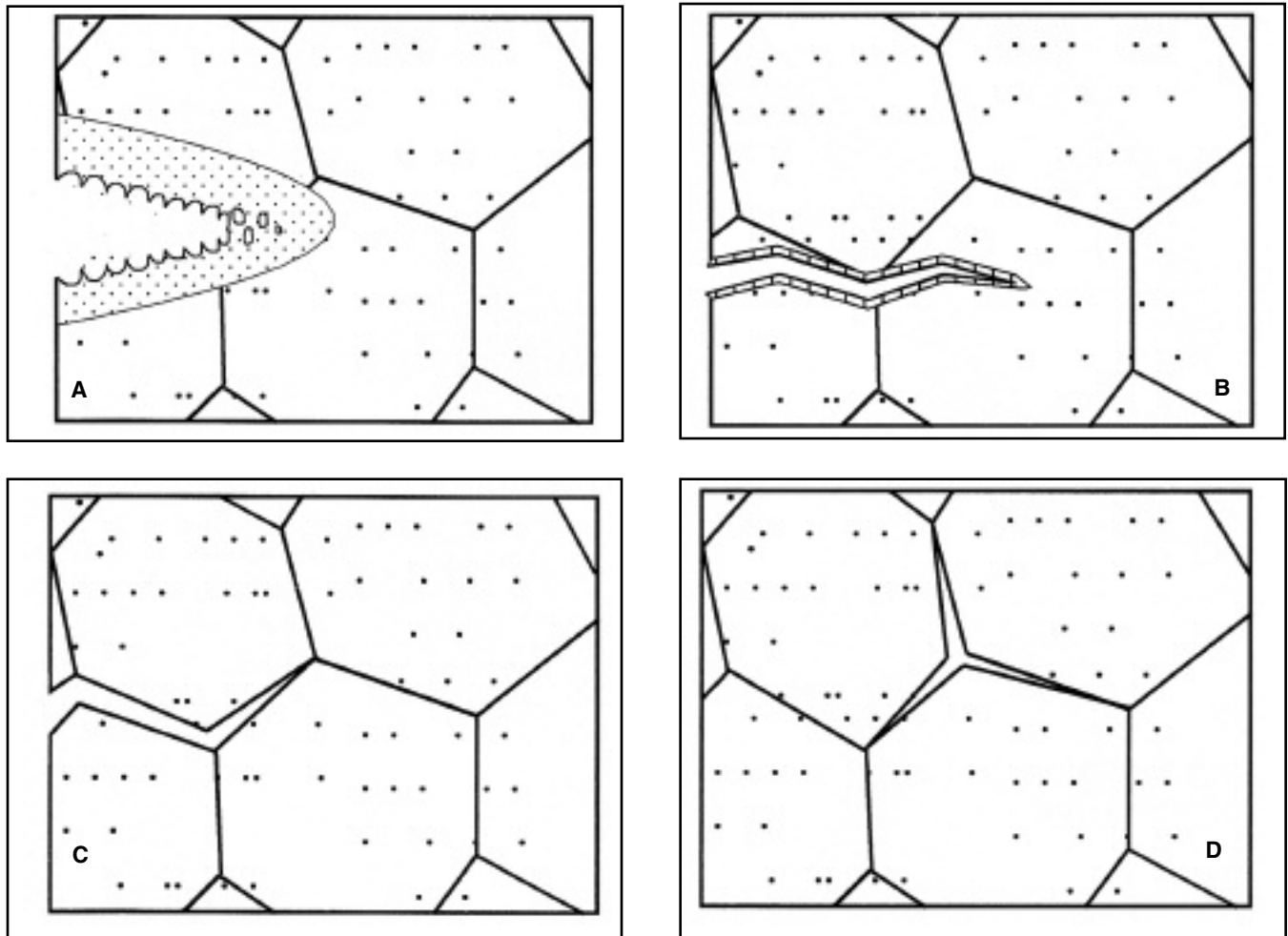


Fig. 8 — Sketches of microscopic fracture modes.

pp. 230, 231. Miami, Fla.: American Welding Society.

3. Signes, E. G., and Howe, P. 1988. Hydrogen assisted cracking in high-strength pipeline steel. *Welding Journal* 67(8): 163-s to 170-s.

4. Suzuki, H. 1978. Cold cracking and its prevention in steel welding. *Transactions of the Japan Welding Society*: 82–86.

5. Hart, M. H. P. 1986. Resistance to hydrogen cracking in steel weld metals. *Welding Journal* 65(1): 14-s to 22-s.

6. Yurioka, N., and Suzuki, H. 1990. Hydrogen assisted cracking in C-Mn and low alloy steel weldments. *International Materials Reviews* 35(4): 217–249.

7. Dolby, R. E. 1977. The weldability of low carbon structure steels. *Welding Institute Research Bulletin* 18(8): 209–216.

8. Mota, J. M. F., and Apps, R. L. 1982. Chevron cracking — A new form of hydrogen cracking in steel weld metals. *Welding Journal* 61(7): 222-s to 228-s.

9. Allen, D. J., Chew, B., and Harris, P. 1982. The formation of chevron cracks in submerged arc weld metal. *Welding Journal* 61(7): 212-s to 221-s.

10. Simcoe, R., Elsea, A. R., and Manning, G. K. 1956. Further work on the boron-hardenable mechanism. *Journal of Metals* 8: pp.

984–988.

11. Maitrepierre, Ph., Thivellier, D., and Tricot, R. 1975. Influence of boron on the decomposition of austenite in low carbon alloyed steels. *Metallurgical Transactions* 6A: pp. 287–321.

12. Pargeter, R. J., and Dolby, R. E. 1985. Guidelines for classification of ferritic steel weld metal microstructural constituents using the light microscope. IIW Doc. IX-1377-85

13. Oh, D. W., Olson, D. L., and Frost, R. H. 1998. The influence of boron and titanium on low-carbon steel weld metal. *Welding Journal* 68: 151-s to 158-s.

14. Ohmori and Yamanaka. 1979. Proceedings of International Symposium on Boron Steel, Milwaukee, Wis. pp. 44–60.

15. Ito, K., and Bessyo, K. 1968. Cracking parameter of high strength steels related to heat-affected zone cracking. *JWS* 37(9): 983–991.

16. Keville, B. R. 1976. An investigation to determine the mechanism involved in the formation and propagation of chevron cracks in submerged arc weldments. *Welding Research International* 6(6): 47–66.

17. Lee, H. W., Kang, S. W., and Um, D. S. 1998. A study on transverse weld cracks in thick steel plate with the FCAW process. *Welding*

Journal 77(12): 503-s to 510-s.

18. Lee, H. W., and Kang, S. 2003. The relationship between residual stresses and transverse weld cracks in thick steel plate. *Welding Journal* 77(12): 225-s to 230-s.

19. Beachem, C. D. 1972. A new model for hydrogen-assisted cracking. *Metallurgical Transactions* 3(2): 437–451.

Change of Address? Moving?

Make sure delivery of your *Welding Journal* is not interrupted. Contact the Membership Department with your new address information — (800) 443-9353, ext. 217; smateo@aws.org.